Published in : C. Walber et al. (eds.), Sensors & Instrumentation and Aircraft/Aerospace Testing Techniques, Volume 8, Conference Proceedings of the Society for Experimental Mechanics Series (2024), pp. 91–97
DOI: 10.1007/978-3-031-34938-6_11
Status : Postprint (Author's version)

REALIZATION OF A VIRTUAL ACOUSTIC BLACK HOLE WITH PIEZOELECTRIC PATCHES

Samuel Quaegebeur[1], Ghislain Raze[1], Li Cheng[2], and Gaëtan Kerschen[1]

[1] Aerospace and Mechanical Engineering Department, University of Liège, Liège, Belgium
[2] Department of Mechanical Engineering, The Hong Kong Polytechnic University Hung Hom, Kowloon, Hong Kong SAR

KEYWORDS: Acoustic black hole • Active control • Vibration reduction • Piezoelectric • Dynamic substructuring

ABSTRACT

Reducing the mechanical vibration is of the utmost importance to lower mechanical stress and thus extend the life of a structure. This work proposes a novel concept to achieve this through an acoustic black hole (ABH) effect implemented via a digital controller. An ABH is a device that localizes the vibrational energy, which is in turn dissipated using damping layers. Its practical realization consists of a tapered wedge beam whose thickness follows a power-law profile. Its efficiency usually starts beyond a cut-on frequency, which is inversely proportional to its length. Obtaining the ABH effect on slender structures is thus very challenging: to achieve vibration reduction at low frequencies, the tapered wedge beam must be very long and thin. We propose herein to circumvent this problem by using a digital controller connected to piezoelectric transducers which are bonded to the host structure. Digital controllers have the significant advantage of being able to reproduce virtually any desired mechanical impedance function and, in particular, that of an ABH. We verify the soundness of the approach through detailed numerical simulations. Those are conducted on a one-dimensional slender beam modeled by the finite element method. The simulations show promising results, and the practical realization of the virtual acoustic black hole (VABH) is discussed eventually.

Published in : C. Walber et al. (eds.), Sensors & Instrumentation and Aircraft/Aerospace Testing Techniques, Volume 8, Conference Proceedings of the Society for Experimental Mechanics Series (2024), pp. 91–97
DOI: 10.1007/978-3-031-34938-6_11
Status : Postprint (Author's version)

11.1 Introduction

The acoustic black hole effect [1] has been the subject of many innovations for the past two decades [2]. This device is obtained by changing the thickness of a profile into a power-law function. The vibrational energy then gets localized inside it, and different strategies can be employed to mitigate the vibrations [3, 4]. However, the ABH effect is efficient above a cut-on frequency which is inversely proportional to the length of the profile. To reduce vibration at low frequencies, very long and thus thin profiles must be manufactured which is very challenging. Some strategies [5, 6] have been developed over the years to enhance the ABH effect without modifying its profile. However, the efficiency of such approaches remains limited and is not as good as if one could create a very long and thin profile.

Piezoelectric shunts [7, 8] correspond to another approach to mitigate vibrations. Attaching a piezoelectric patch to a host enables to convert mechanical energy into electrical energy. Connecting the patch to a shunt (for instance, a resonant shunt) enables to dissipate the energy and thus to reduce the vibrations. However, the components forming the shunt may be difficult to create in practice or ill-adapted. Digital vibration absorbers (DVAs) [9] allow to circumvent this problem. Instead of plugging a passive electrical circuit to the piezoelectric patches, it is connected to a digital unit and a source of power to reproduce any electrical impedance function. These systems are thus very versatile and are used for a wide range of applications such as nonlinear vibration [10].

The key idea of this research is to propose a physical implementation of a VABH. Such a concept enables to tackle any practical issues encountered with ABH and to create designs that could never be obtained in practice.

11.2 Background

Figure 11.1 presents the mechanical structure under study. All parameters of the system are provided in Table 11.1. While the uniform beam has a constant thickness h_0, the tapered wedge beam's profile satisfies the following law:

$$h(x) = h_0 \left(\frac{L+L_{ABH}-x}{L_{ABH}}\right)^m, x \in [L, L + L_{ABH} - x_0] \tag{11.1}$$

where x_0 denotes the tapered wedge beam truncation. The beam is clamped at its extremity $x = 0$ and free at the tip. The cut-on frequency of the device [11] is equal to 40.9 Hz.

The system is discretized with the finite element method. Each node is characterized by three displacements: the longitudinal and transversal displacements and the rotational displacement. Superscripts b and tb denote the uniform and tapered wedge beams, respectively. For both systems, the internal nodes are noted by the subscript I and the boundary nodes (nodes shared by both beams) by B. The equations of motion of both systems read

Published in : C. Walber et al. (eds.), Sensors & Instrumentation and Aircraft/Aerospace Testing Techniques, Volume 8, Conference Proceedings of the Society for Experimental Mechanics Series (2024), pp. 91–97
DOI: 10.1007/978-3-031-34938-6_11
Status : Postprint (Author's version)

$$\begin{bmatrix}\mathbf{M}_{\mathrm{II}}^{\mathrm{b}} \mathbf{M}_{\mathrm{IB}}^{\mathrm{b}} \\ \mathbf{M}_{\mathrm{BI}}^{\mathrm{b}} \mathbf{M}_{\mathrm{BB}}^{\mathrm{b}}\end{bmatrix}\begin{bmatrix}\ddot{\mathbf{x}}_{\mathrm{I}}^{\mathrm{b}} \\ \ddot{\mathbf{x}}_{\mathrm{B}}\end{bmatrix}+\begin{bmatrix}\mathbf{C}_{\mathrm{II}}^{\mathrm{b}} \mathbf{C}_{\mathrm{IB}}^{\mathrm{b}} \\ \mathbf{C}_{\mathrm{BI}}^{\mathrm{b}} \mathbf{C}_{\mathrm{BB}}^{\mathrm{b}}\end{bmatrix}\begin{bmatrix}\dot{\mathbf{x}}_{\mathrm{I}}^{\mathrm{b}} \\ \dot{\mathbf{x}}_{\mathrm{B}}\end{bmatrix}+\begin{bmatrix}\mathbf{K}_{\mathrm{II}}^{\mathrm{b}} \mathbf{K}_{\mathrm{IB}}^{\mathrm{b}} \\ \mathbf{K}_{\mathrm{BI}}^{\mathrm{b}} \mathbf{K}_{\mathrm{BB}}^{\mathrm{b}}\end{bmatrix}\begin{bmatrix}\mathbf{x}_{\mathrm{I}}^{\mathrm{b}} \\ \mathbf{x}_{\mathrm{B}}\end{bmatrix}=\begin{bmatrix}\mathbf{f}_{\mathrm{ext,I}} \\ \mathbf{f}_{\mathrm{ext,B}}+\mathbf{f}_{\mathrm{tb}\to\mathrm{b}}\end{bmatrix} \tag{11.2a}$$

$$\begin{bmatrix}\mathbf{M}_{\mathrm{II}}^{\mathrm{tb}} \mathbf{M}_{\mathrm{IB}}^{\mathrm{tb}} \\ \mathbf{M}_{\mathrm{BI}}^{\mathrm{tb}} \mathbf{M}_{\mathrm{BB}}^{\mathrm{tb}}\end{bmatrix}\begin{bmatrix}\ddot{\mathbf{x}}_{\mathrm{I}}^{\mathrm{tb}} \\ \ddot{\mathbf{x}}_{\mathrm{B}}\end{bmatrix}+\begin{bmatrix}\mathbf{C}_{\mathrm{II}}^{\mathrm{tb}} \mathbf{C}_{\mathrm{IB}}^{\mathrm{tb}} \\ \mathbf{C}_{\mathrm{BI}}^{\mathrm{tb}} \mathbf{C}_{\mathrm{BB}}^{\mathrm{tb}}\end{bmatrix}\begin{bmatrix}\dot{\mathbf{x}}_{\mathrm{I}}^{\mathrm{tb}} \\ \dot{\mathbf{x}}_{\mathrm{B}}\end{bmatrix}+\begin{bmatrix}\mathbf{K}_{\mathrm{II}}^{\mathrm{tb}} \mathbf{K}_{\mathrm{IB}}^{\mathrm{tb}} \\ \mathbf{K}_{\mathrm{BI}}^{\mathrm{tb}} \mathbf{K}_{\mathrm{BB}}^{\mathrm{tb}}\end{bmatrix}\begin{bmatrix}\mathbf{x}_{\mathrm{I}}^{\mathrm{tb}} \\ \mathbf{x}_{\mathrm{B}}\end{bmatrix}=\begin{bmatrix}\mathbf{0} \\ -\mathbf{f}_{\mathrm{tb}\to\mathrm{b}}\end{bmatrix} \tag{11.2b}$$

where $\mathbf{M}$, $\mathbf{C}$, and $\mathbf{K}$ correspond to the mass, damping, and stiffness matrices. External forces, $\mathbf{f}_{\mathrm{ext}}$, are applied to the uniform beam, but we assume that none of them are applied to the tapered wedge beam. Both beams share a boundary where internal forces, $f_{tb\to b}$, are transmitted. This term translates the ABH effect on the uniform beam. Using the Laplace transform, with s its variable, in Equation (11.2b), gives

$$\mathbf{X}_{\mathrm{I}}=\underbrace{\left(s^2\mathbf{M}_{\mathrm{II}}^{\mathrm{tb}}+s\mathbf{C}_{\mathrm{II}}^{\mathrm{tb}}+\boldsymbol{K}_{\mathrm{II}}^{\mathrm{tb}}\right)^{-1}\left(s^2\mathbf{M}_{\mathrm{IB}}^{\mathrm{tb}}+s\mathbf{C}_{\mathrm{IB}}^{\mathrm{tb}}+\mathbf{K}_{\mathrm{IB}}^{\mathrm{tb}}\right)}_{\mathbf{Z}_{\mathrm{IB}}(s)}\mathbf{X}_{\mathrm{B}} \tag{11.3a}$$

$$-\mathbf{f}_{\mathrm{tb}\to\mathrm{b}}=\underbrace{\left[\left(s^2\mathbf{M}_{\mathrm{II}}^{\mathrm{tb}}+s\mathbf{C}_{\mathrm{II}}^{\mathrm{tb}}+\mathbf{K}_{\mathrm{II}}^{\mathrm{tb}}\right)^{-1}\left(s^2\mathbf{M}_{\mathrm{BB}}^{\mathrm{tb}}+s\mathbf{C}_{\mathrm{BB}}^{\mathrm{tb}}+\mathbf{K}_{\mathrm{BB}}^{\mathrm{tb}}\right)\right]}_{\mathbf{Z}_{\mathrm{ABH}}(s)}\mathbf{X}_{\mathrm{B}} \tag{11.3b}$$

where $\mathbf{X}_{\mathrm{I}}$, $\mathbf{X}_{\mathrm{B}}$, and $\mathbf{X}_{\mathrm{tb}\to\mathrm{b}}$ are the Laplace transforms of $\mathbf{x}_{\mathrm{I}}^{\mathrm{tb}}$, $\mathbf{x}_{\mathrm{b}}$, and $\mathbf{x}_{\mathrm{tb}\to\mathrm{b}}$.

For fast computation and efficiency, it is convenient to reduce the finite element models with a Craig-Bampton reduction [12]. Boundary nodes are kept as master nodes, and a sufficient number of modes are kept in the basis to have very good accuracy within the excitation frequency range [0Hz, 2kHz]. Moreover, the evaluation of (11.3b) can also be computed through a state-space formulation [13] for simplicity.

In the active control terminology, the dynamics of the plant (beam) has a feedback function with a controller (ABH). By measuring the displacement at the boundary ($\mathbf{x_b}$), one can actuate the forces $\mathbf{f}_{\mathrm{tb}\to\mathrm{b}}$ to mimic the effect of the physical ABH. This process is illustrated in Fig. 11.2.

To reproduce exactly the ABH effect, all displacements of the boundary must be captured, and all forces need to be applied. This constitutes a limitation to the active control approach as no device can apply at the same point both independent forces and a torque. Therefore, in the following, the approach will measure the rotation at the boundary and apply a torque to reproduce the rotation effect of the ABH.

Figure 11.1 *Representation of a beam with a tapered wedge profile*

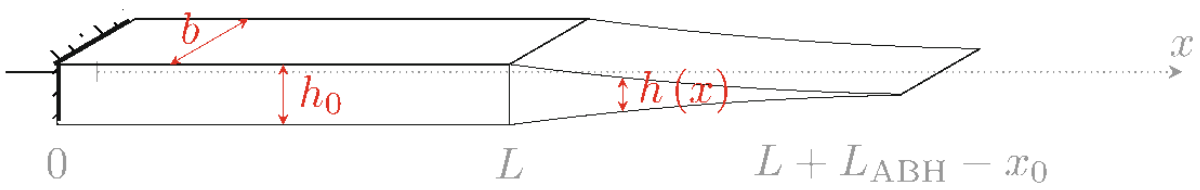

Published in : C. Walber et al. (eds.), Sensors & Instrumentation and Aircraft/Aerospace Testing Techniques, Volume 8, Conference Proceedings of the Society for Experimental Mechanics Series (2024), pp. 91–97
DOI: 10.1007/978-3-031-34938-6_11
Status : Postprint (Author's version)

Table 11.1 *Parameters of the mechanical system*

Parameter	*Beam*	*ABH*	*Piezoelectric patch*
Length	$L = 700$ *mm*	$L_{ABH} = 700$ *mm*	*67.5 mm*
Width (b)	*14 mm*	*14 mm*	*14 mm*
Thickness	$h_0 = 14$ *mm*	$m = 2, x_0 = 10$ *mm*	*2 mm*
Young modulus	$E_b = 210$*GPa*	$E_{ABH} = 210$*GPa*	*66GPa*
Density	ϱ_b=7800 kg m^{-3}	ϱ_{ABH} =7800 kg m^{-3}	7800kgm^{-3}
Damping	$\xi_b = 0.05\%$	$\xi_{ABH} = 5\%$	

Figure 11.2 *Block diagram of the system*

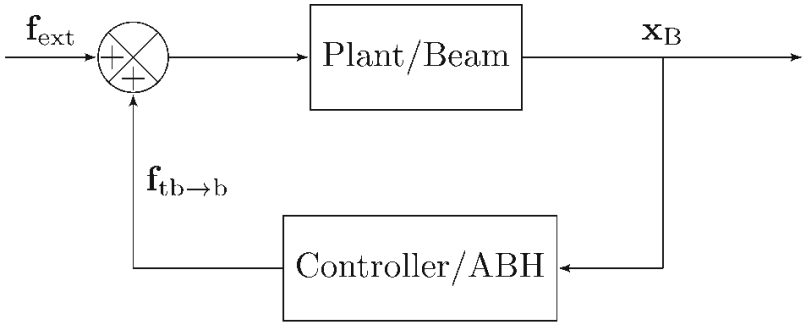

Figure 11.3 *Illustration of the piezoelectric patch on a portion of the beam*

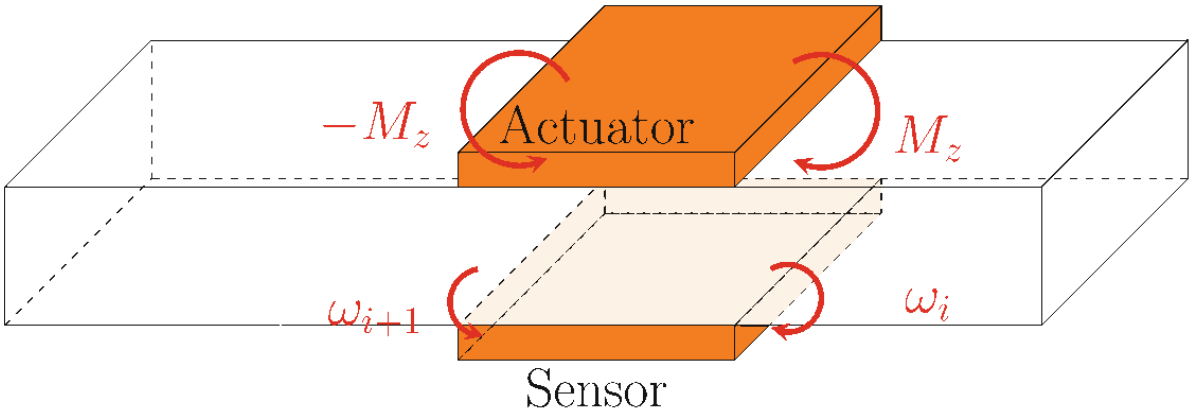

11.3 Analysis

The rotational effect of the ABH is achieved with a rectangular piezoelectric patch [14]. Figure 11.3 illustrates a collocated pair on a portion of a beam. Due to the deformation of the structure, the sensor patch will provide a current $\dot{q}_s$ from which the rotation ω can be retrieved. The signal is then processed by the digital unit and a voltage will be delivered to the actuator patch V_a. Finally, this voltage will create a moment at the boundaries and thus reproduce the rotational effect of the ABH.

Published in : C. Walber et al. (eds.), Sensors & Instrumentation and Aircraft/Aerospace Testing Techniques, Volume 8, Conference Proceedings of the Society for Experimental Mechanics Series (2024), pp. 91–97
DOI: 10.1007/978-3-031-34938-6_11
Status : Postprint (Author's version)

However, a rectangular piezoelectric patch creates two moments: one at each of its boundaries. Based on the theory presented in the previous section, the ABH rotational effect should only be applied to the extremity of the beam. To remedy this issue, a first idea would be to create a very long patch which covers the entire length of the beam. The correct ABH torque could be applied at the free tip, and the additional torque would be applied to the clamped side and hence will not impact the result.

In practice, very long patches are not convenient. Another solution would be to consider multiple adjacent patches one beside the other to cover the length of the beam. The patch at the free tip will reproduce the ABH effect, while its neighbour will create a torque to compensate the additional torque created by the first patch, and so on. This approach is detailed next theoretically.

We consider a beam composed of N pairs of identical collocated piezoelectric patches, see Fig. 11.4. Each pair is adjacent in order to cover the entire length of the beam. In one pair, as shown in Fig. 11.3, one piezoelectric patch is actuating the structure, whereas the other is sensing its response. This sensor is assumed to be connected to a perfect current sensing device and is thus considered to be in short circuit $(V_{i,s} = 0)$. The equations of motion of the system are

Figure 11.4 *Beam covered with N pairs of collocated piezoelectric patches*

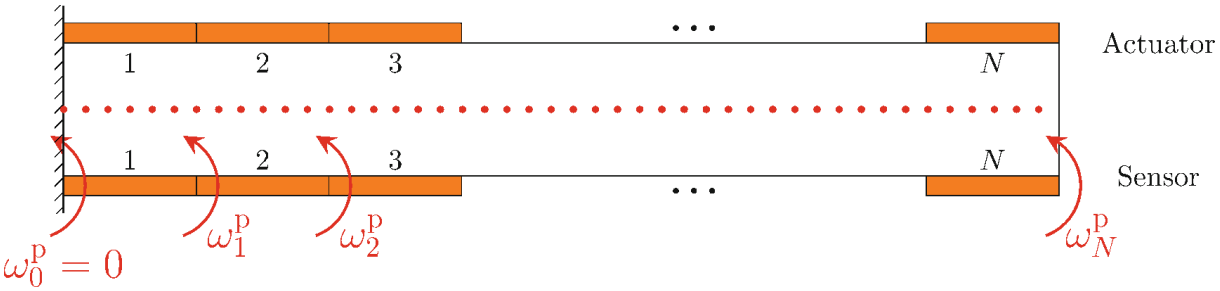

$$\begin{cases} \mathbf{M}\ddot{\mathbf{x}} + \mathbf{C}\dot{\mathbf{x}} + \mathbf{K}_{\mathrm{sc}}\mathbf{x} + \sum_{i=1}^{N}\left(\mathbf{\Theta}_i C^{\varepsilon} V_{i,a}\right) = \mathbf{F} \\ \mathbf{\Theta}_i^T\mathbf{x} - (C^{\varepsilon})^{-1} q_{i,a} = V_{i,a}, \forall i \in [\![1, N]\!] \\ C^{\varepsilon}\mathbf{\Theta}_i^T\mathbf{x} = q_{i,s}, \qquad \forall i \in [\![1, N]\!] \end{cases} \tag{11.4}$$

The scalar C^{ε} represents the capacitance at constant strain of the piezoelectric patches. The vector $\mathbf{x}$ contains the displacements of all degrees of freedom (of size 3 x N_{nodes}),

$$\mathbf{x} = \left[u_1, v_1, \omega_1, \dots, u_j, v_j, \omega_j, \dots, u_k, v_k, \omega_k, \dots, u_{N_{nodes}}, v_{N_{nodes}}, \omega_{N_{nodes}}\right]^T \tag{11.5}$$

where j and k are two arbitrary nodes. The matrix $\mathbf{\Theta}_i$ is the i-th piezoelectric patch coupling vector. Assuming that the boundaries of the i-th piezoelectric patch are connected to the nodes j and k, we have (following the same layout as Equation (11.5))

$$\mathbf{\Theta} = \theta[0,0,0, \dots, 0,0, -1, \dots, 0,0,1, \dots, 0,0,0]^T \tag{11.6}$$

with θ a piezoelectric constant equal for all patches. The matrix $\mathbf{K}_{\mathrm{sc}}$ is the stiffness matrix of the short-circuited system. The finite element method [15] is employed to compute all the quantities (dynamics of the piezoelectric patches accounted for).

Published in : C. Walber et al. (eds.), Sensors & Instrumentation and Aircraft/Aerospace Testing Techniques, Volume 8, Conference Proceedings of the Society for Experimental Mechanics Series (2024), pp. 91–97
DOI: 10.1007/978-3-031-34938-6_11
Status : Postprint (Author's version)

In the following, ω_i^p denotes the rotation of the right boundary of the i-th piezoelectric patch as depicted in Fig. 11.4.

The voltage applied to the structure $V_{i,a}$ is specified by the impedance Z_i implemented in the digital unit. In the Laplace domain, we have

$$\begin{aligned} V_{i,a} &= Z_i(s)Q_{i,s} \\ &= Z_i(s)C^\varepsilon \boldsymbol{\Theta}_I^T \mathbf{X} \\ &= Z_i(s)C^\varepsilon\theta\left(\Omega_i^p - \Omega_{i-1}^p\right) \end{aligned} \tag{11.7}$$

where Q, $\mathbf{X}$, and Ω^p are the Laplace transform of q, $\mathbf{x}$, and ω^p, respectively. Substituting this equation in the dynamics of the beam (first equation of (11.4)) and equating the result to the dynamics of the beam with ABH (see Equation (11.2a)), we have the following equations to satisfy:

$$\begin{aligned} &(C^\varepsilon\theta)^2 Z_N\left(\Omega_N^p - \Omega_{N-1}^p\right) = -\mathbf{Z}_{ABH}\Omega_N^p \\ &(C^\varepsilon\theta)^2 Z_i\left(\Omega_N^p - \Omega_{N-1}^p\right) = (C^\varepsilon\theta)^2 Z_{i+1}\left(\Omega_{i+1}^p - \Omega_i^p\right) \quad \forall i \in [\![1, N-1]\!] \end{aligned} \tag{11.8}$$

with $\Omega_0^p = 0$ and Z_{ABH} the rotational part of $\mathbf{Z}_{ABH}$ defined in Equation (11.3b). The first equation translates the ABH effect to reproduce. The second equation corresponds to torques created by two adjacent patches which need to be cancelled out. The solution of the previous system is

$$Z_I = \frac{-\mathbf{Z}_{ABH}}{(C^\varepsilon\theta)^2}\left(\frac{\Omega_N^p}{\Omega_i^p - \Omega_{i-1}^p}\right) \quad \forall i \in [\![1, N]\!] \tag{11.9}$$

Summing the measured current (see the third part of Equation (11.4)) gives

$$\Omega_N^p = \frac{1}{(C^\varepsilon\theta)}\sum_{i=1}^n Q_{i,s} \tag{11.10}$$

Finally, the impedance of (11.9) is equal to

$$Z_I = \frac{-\mathbf{Z}_{ABH}}{(C^\varepsilon\theta)^2 q_{i,s}}\sum_{i=1}^N q_{i,s} \quad \forall i \in [\![1, N]\!] \tag{11.11}$$

In the end, the voltage that needs to be applied to the piezoelectric patch is equal to

$$\begin{aligned} V_{i,a} &= Z_i q_{i,s} \\ &= \frac{-\mathbf{Z}_{ABH}}{(C^\varepsilon\theta)^2}\sum_{i=1}^N q_{i,s} \end{aligned} \tag{11.12}$$

Therefore, in practice, the sum of the currents is measured (which can be achieved by connecting the sensors in parallel), the function $\frac{-\mathbf{Z}_{ABH}}{(C^\varepsilon\theta)^2}$ is implemented in the digital unit, and the actuation voltage, being identical for every actuator, is applied in parallel to them.

The proposed approach is now validated numerically. Ten pairs of piezoelectric patches are attached to the structure. The geometry and material are provided in Table 11.1. The capacitance C^ε is equal to 25 nF. The vector $\boldsymbol{\Theta}$ is obtained with the finite element method [15]. A transversal excitation is applied at 65% of the beam, and the transversal displacement of the tip is observed.

In practice, gaps (of length 2.5 mm) exist between the patches, and thus the torques at boundaries do not cancel each other out perfectly: a residual moment exists. To study the influence of the VABH, four simulations are proposed: the beam itself, the beam with the full ABH effect, the beam

Published in : C. Walber et al. (eds.), Sensors & Instrumentation and Aircraft/Aerospace Testing Techniques, Volume 8, Conference Proceedings of the Society for Experimental Mechanics Series (2024), pp. 91–97
DOI: 10.1007/978-3-031-34938-6_11
Status : Postprint (Author's version)

with the VABH when no gap exists between the piezoelectric patches (ideal VABH), and finally the beam with VABH with gaps between the patches (realistic VABH). The discretization in the finite element model is such that nodes exist within the gaps. The results are presented in Fig. 11.5. When the ABH effect is taken into account (full one or digital), vibration reduction is obtained. Only the first mode at 24.5 Hz (below the cut-on frequency) is not well attenuated. Similar trends exist between the full ABH and the VABH: vibration mitigation is obtained after the cut-on frequency, and the resonant frequencies of the system are shifted to low frequencies. The VABH with realistic gaps provides very close results to the VABH without gap.

Overall, these results give very good confidence in achieving vibration reduction with VABH.

To show the versatility of our approach, we now create a VABH with a length of 1400 mm (and thus a cut-on frequency of 10 Hz) and a modal damping of 50%. The results are shown in Fig. 11.6. With the longer tapered wedge beam and the higher modal damping, all peaks are very well attenuated.

Figure 11.5 *Frequency forced response with multiple piezoelectric patches. The vertical dashed black line represents the cut-on frequency*

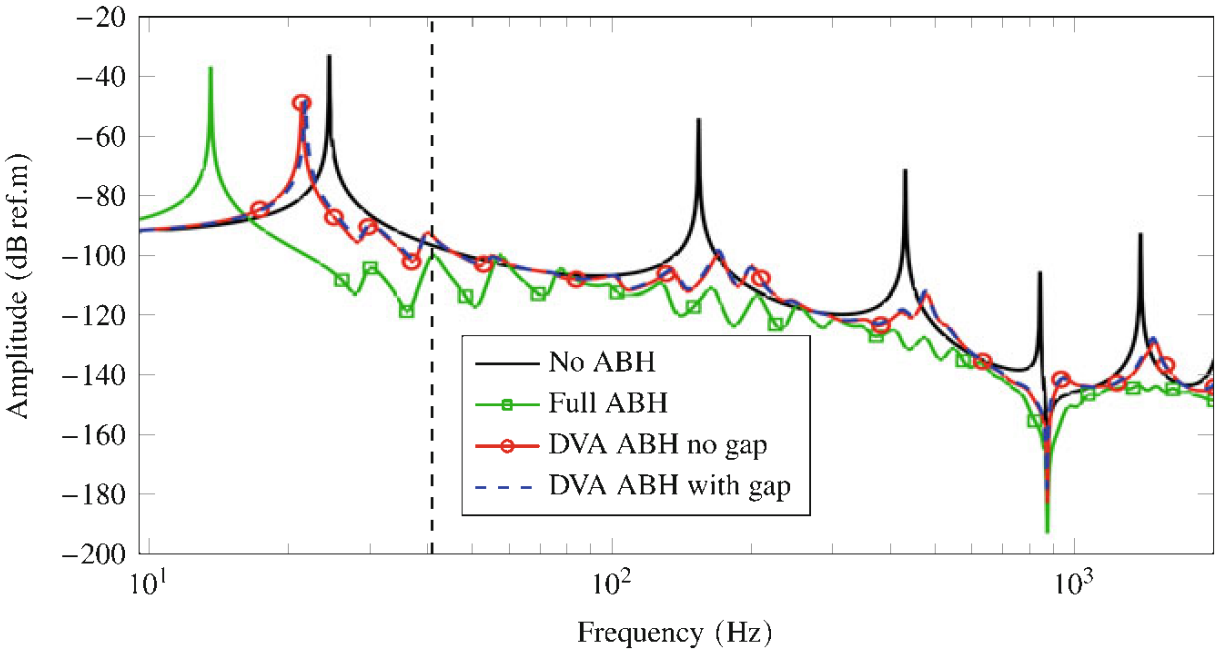

Published in : C. Walber et al. (eds.), Sensors & Instrumentation and Aircraft/Aerospace Testing Techniques, Volume 8, Conference Proceedings of the Society for Experimental Mechanics Series (2024), pp. 91–97
DOI: 10.1007/978-3-031-34938-6_11
Status : Postprint (Author's version)

Figure 11.6 *Frequency forced response with a longer ABH*

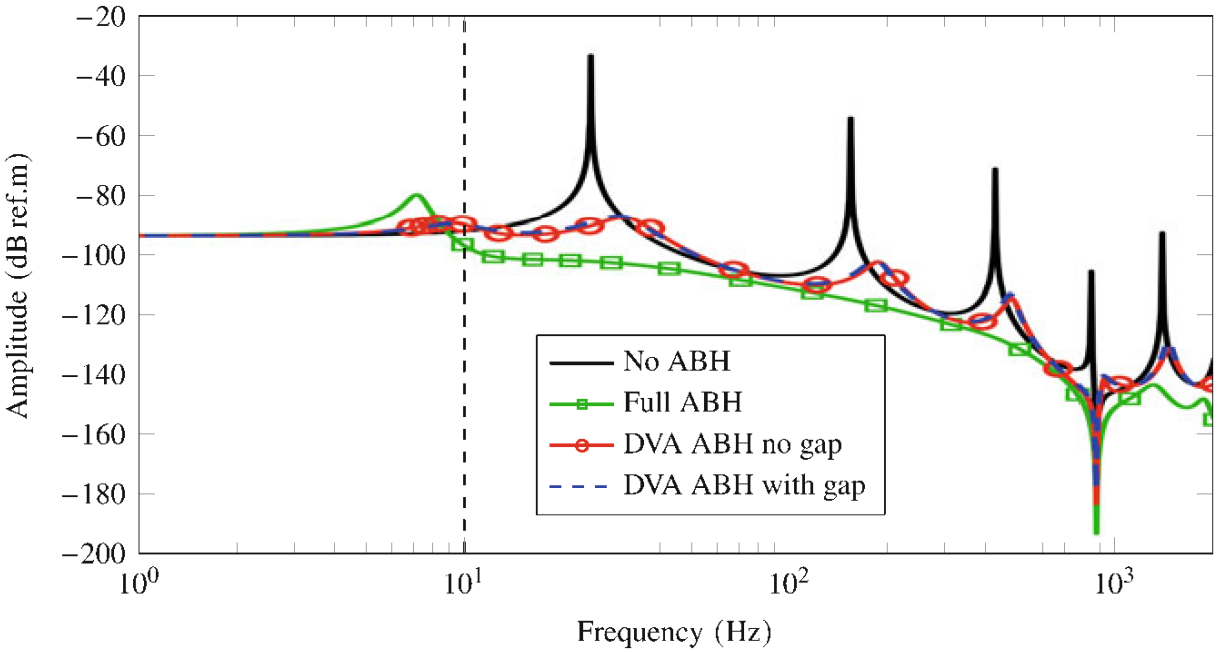

11.4 Conclusion

This chapter presents the combination of the acoustic black hole effect with digital controllers to create for the first time a VABH. Piezoelectric patches were employed to realize this device. As the ABH consists in applying appropriate boundary conditions at the tip of the beam, multiple patches were considered to achieve this properly. The electromechanical equations of motion were presented and the mechanical impedance that needs to be implemented in the controller was derived.

The concept was then tested numerically, and excellent performance was observed. Besides, an ABH not realizable in practice was implemented successfully in the digital controller. The perspective of this work would be the experimental validation of these results.

Acknowledgments This research is supported by a grant from the Belgian National Science Foundation (FRS-FNRS PDR T.0124.21), which is gratefully acknowledged.

Published in : C. Walber et al. (eds.), Sensors & Instrumentation and Aircraft/Aerospace Testing Techniques, Volume 8, Conference Proceedings of the Society for Experimental Mechanics Series (2024), pp. 91–97
DOI: 10.1007/978-3-031-34938-6_11
Status : Postprint (Author's version)

References

1. Mironov, M.: Propagation of a flexural wave in a plate whose thickness decreases smoothly to zero in a finite interval. Sov. Phys. Acoust. **34**, 318-319 (1988)
2. Pelat, A., Gautier, F., Conlon, S.C., Semperlotti, F.: The acoustic black hole: a review of theory and applications. J. Sound Vib. **476**, 115316 (2020)
3. Krylov, V.V., Tilman, F.J.B.S.: Acoustic 'black holes' for flexural waves as effective vibration dampers. J. Sound Vib. **274**(3), 605-619 (2004)
4. Zhang, L., Kerschen, G., Cheng, L.: Electromechanical coupling and energy conversion in a PZT-coated acoustic black hole beam. Int. J. Appl. Mech. **12**(08), 2050095 (2020). World Scientific Publishing Co
5. Denis, V., Pelat, A., Touzé, C., Gautier, F.: Improvement of the acoustic black hole effect by using energy transfer due to geometric nonlinearity. Int. J. Non-Linear Mech. 94, 134-145 (2017)
6. Cheer, J., Hook, K., Daley, S.: Active feedforward control of flexural waves in an Acoustic Black Hole terminated beam. Smart Mater. Struct. **30**(3), 035003 (2021). IOP Publishing
7. Forward, R.L.: Electronic damping of vibrations in optical structures. Appl. Opt. **18**(5), 690-697 (1979). Optica Publishing Group
8. Hagood, N.W., von Flotow, A.: Damping of structural vibrations with piezoelectric materials and passive electrical networks. J. Sound Vib. **146**(2), 243-268 (1991)
9. Fleming, A.J., Behrens, S., Moheimani, S.O.R.: Synthetic impedance for implementation of piezoelectric shunt-damping circuits. Electron. Lett. **36**(18), 1525-1526 (2000). IET Digital Library
10. Raze, G., Jadoul, A., Guichaux, S., Broun, V., Kerschen, G.: A digital nonlinear piezoelectric tuned vibration absorber. Smart Mater. Struct. **29**(1), 015007 (2019). IOP Publishing
11. Aklouche, O., Pelat, A., Maugeais, S., Gautier, F.: Scattering of flexural waves by a pit of quadratic profile inserted in an infinite thin plate. J. Sound Vib. **375**, 38-52 (2016)
12. Craig, R., Bampton, M.: Coupling of substructures for dynamic analyses. AIAA J. **6**(7), 1313-1319 (1968)
13. Preumont, A.: State space approach. In: Preumont, A. (ed.) Vibration Control of Active Structures: An Introduction, 3rd edn. Solid Mechanics and Its Applications, pp. 187-213. Springer, Dordrecht (2011)
14. Preumont, A.: Piezoelectric beam, plate and truss. In: Preumont, A. (ed.) Vibration Control of Active Structures: An Introduction, 3rd edn. Solid Mechanics and Its Applications, pp. 61-101. Springer, Dordrecht (2011)
15. Thomas, O., Deü, J.-F., Ducarne, J.: Vibrations of an elastic structure with shunted piezoelectric patches: efficient finite element formulation and electromechanical coupling coefficients. Int. J. Numer. Methods Eng. **80**(2), 235-268 (2009)